IMPROVED SUBPIXEL MONITORING OF SEASONAL SNOW COVER: A CASE STUDY IN THE ALPS

M.A. Veganzones[1,3], M. Dalla Mura[1], M. Dumont[2], I. Zin[3], J. Chanussot[1,4]

[1]GIPSA-lab, Grenoble-INP, Saint Martin d'Hères, France
[2]Météo-France-CNRS, CNRM-GAME/CEN, UMR 3589, Saint Martin d'Hères, France
[3]LTHE, Grenoble-INP, Saint Martin d'Hères, France
[4]Faculty of Electrical and Computer Engineering, University of Iceland, Reykjavik, Iceland
GIPSA-lab, LTHE and MeteoFrance are part of Labex OSUG@2020 (ANR10 LABX56)

ABSTRACT

The snow coverage area (SCA) is one of the most important parameters for cryospheric studies. The use of remote sensing imagery can complement field measurements by providing means to derive SCA with a high temporal frequency and covering large areas. Images acquired by the Moderate Resolution Imaging Spectroradiometer (MODIS) are perhaps the most widely used data to retrieve SCA maps. Some MODIS derived algorithms are available for subpixel SCA estimation, as MODSCAG and MODImLab. Both algorithms make use of spectral unmixing techniques using a fixed set of snow, rocks and other materials spectra (endmembers). We aim to improve the performance of a modified version of MODImLab algorithm by exploring advanced spectral unmixing techniques. Furthermore, we make use of endmember induction algorithms to obtain the endmembers from the data itself instead of using a fixed spectral library. We validate the proposed approach on a case study in the mountainous region of the Alps.

***Index Terms*—** Snow coverage area, SCA, spectral unmixing, MODIS, Alps.

1. INTRODUCTION

The snow coverage area (SCA) is one of the most important parameters for cryospheric studies [1]. The amount of snow fallen on the surface is of fundamental importance for studies in many fields such as hydrology (for the retrieval of the snow water equivalent, or flood forecasting), energy (estimations of the expected hydroelectric power), glaciology (for estimation of mass balances of glaciers) and climate change studies (detection of anomalies and trends in the evolution of the snow coverage over the years due to climate fluctuations). The estimation of the SCA is usually conducted using field measurements, either manual surveys or automatic weather stations on the ground. Although this approach leads to accurate measurements, these are limited to local scale and do not provide data with a large spatial coverage. Remote sensing imagery can complement these measurements by providing means to derive SCA with a high temporal frequency and covering large areas through the analysis of the acquired imagery.

Among all the remote sensing products, images acquired by the Moderate Resolution Imaging Spectroradiometer (MODIS) are perhaps the most widely used data to retrieve SCA maps. MODIS is an imaging sensor aboard the Terra and Aqua satellites, which are viewing the entire Earths surface every one to two days, acquiring data in 36 spectral bands[1]. The MODIS snow products include the MODIS fractional snow cover based on spectral unmixing (MODSCAG) [2]. The MODSCAG product assumes that the measured reflectance of each pixel is given by a linear mixture of a set of pure spectra (e.g., snow, ice, vegetation, and rocks), which are called endmembers. Although the MODSCAG product has proved to be more accurate than the methods based on the normalized difference snow index [3, 4], its wide application is limited by the selection of the endmembers. Currently, these are fixed and do not comprehensively account for the different states of the snow surface (e.g., dirty snow is not accounted, [7]). The MODImLab algorithm introduced in [5], corrects the reflectance values by considering topographic and atmospheric effects, and obtains the SCA with the algorithm described in [6] which performs a spectral unmixing on a set of images at 250m by fusing the reflectance bands at 500m with the two at 250m. Authors in [7] extended the work in [5] by comparing different retrieval techniques for snow grain size.

Here, we extend the approach in [7] by exploring the application of more advanced spectral unmixing techniques for increasing the precision in retrieving the SCA maps. We address the spectral variability issue by using a (partially) constrained least squares unmixing (CLSU) algorithm. Furthermore, we make use of endmember induction algorithms to induce the endmembers from the data instead of using a fixed

[1]http://modis.gsfc.nasa.gov

spectral library. By adapting the endmembers to the data we expect to improve the unmixing results while still being capable of identifying the different snow conditions. Experimental validation will be provided through a case study in the mountainous region of the Alps.

The remainder of the paper is as follows. In Sec. 2, an overview of spectral unmixing is given. In Sec. 3, advanced spectral unmixing techniques and the induction of endmembers from data are presented. In Sec. 4, we give experimental validation of the improved subpixel monitoring of snow cover by a case study in the region of the Alps. Finally, we provide some conclusions in Sec. 5.

2. SPECTRAL UNMIXING

The Spectral Unmixing (SU) is the process by which a given pixel is decomposed in the spectral signatures of the materials that contains and their fractional abundances. The most common approach relies in the assumption that a pixel is formed by a linear combination of the spectral signatures of pure materials present in the sample (endmembers), normally corresponding to macroscopic objects in scene, plus some additive noise. This is the so-called Linear Mixing Model (LMM). Let $\mathbf{E} = [\mathbf{e}_1, \ldots, \mathbf{e}_m]$ be the pure endmember signatures, where each $\mathbf{e}_i \in \mathbb{R}^q$ is a q-dimensional vector. Then, the LMM states that a pixel signature, $\mathbf{r} \in \mathbb{R}^q$, is defined by the expression:

$$\mathbf{r} = \sum_{i=1}^{m} \mathbf{e}_i \phi_i + \mathbf{n}, \tag{1}$$

where $\boldsymbol{\phi}$ is the m-dimensional vector of fractional per-pixel abundances and $\mathbf{n}$ is an independent additive noise component. Some physical constraints can be enforced regarding the fractional abundances. The Abundance Non-negative Constraint (ANC), $\phi_i \geq 0,\ \forall i$, ensures that there are not materials with negative contributions. The Abundance Sum-to-one Constraint (ASC), $\sum_{i=1}^{m} \phi_i = 1$, makes the total contributions of the materials sum up to one. In this model, the pixels lie inside a simplex whose vertexes are the endmembers.

Given the endmembers, the spectral unmixing aims to estimate their fractional abundances for each pixel independently. This can be modelled as an inversion problem:

$$\hat{\boldsymbol{\phi}} = \arg\min_{\boldsymbol{\phi}} \left\| \mathbf{r} - \sum_{i=1}^{m} \mathbf{e}_i \phi_i \right\|_2 , \tag{2}$$

subject to ANC and ASC abundance constraints. A solution to (2) is given by the full constrained (FC) least squares, which in the spectral unmixing context is known as the FC-least squares unmixing (FCLSU).

3. ADVANCED SPECTRAL UNMIXING AND ENDMEMBERS INDUCTION

3.1. Spectral variability

In real scenarios, the LMM and the fractional abundances estimated by the FCLSU are seriously affected by spectral variabilities due to variable illumination and environmental, atmospheric, and temporal conditions. By ignoring these variations, errors are introduced and propagated through hyperspectral image analysis [8]. A simple way to address spectral variations is by dropping the ASC constraint, and solving (2) by (partially) constrained least squares unmixing (CLSU).

In this model, variabilities can be modelled as a scaling factor, $\lambda > 0$, that affects each endmember at a given pixel:

$$\mathbf{r} = \sum_{i=1}^{m} \mathbf{e}_i \alpha_i \phi_i + \mathbf{n}. \tag{3}$$

In this extended LMM model, the hyperspectral pixels lie inside the positive hypercone defined by the endmembers. The CLSU implements the extended LMM (3) by solving the following inversion problem, $\mathbf{r} = \sum_{i=1}^{m} \mathbf{e}_i a_i + \mathbf{n}$, where the estimated weighting factors, a_i, are ANC but not ASC. The estimated weighting factors incorporate the information from the spectral abundances, θ_i and the scaling factors, α_i, that is, $a_i = \alpha_i \phi_i$. In order to retrieve the fractional abundances, it is possible to assume that the scaling factor is the same for all the endmembers, $\alpha_i = \alpha, \forall i$, and estimate it as $\alpha = \sum_{i=1}^{m} a_i$. Then, the fractional abundances are obtained by normalizing the vector of weighting factors by the estimated scaling factor, $\phi_i = a_i / \alpha$.

3.2. Endmembers induction algorithms

Most of the times, the spectral signatures of the materials are unknown, and the set of endmembers must be built by either selecting spectral signatures from a spectral library, or by inducing them from the image itself. Both can be performed manually or in an automatic way. In order to automatically induce the set of endmembers from the image, the use of some endmember induction algorithm (EIA) is required. The hyperspectral literature features plenty of such algorithms [9].

Among them, algorithms exploiting the geometrical characteristics of the LMM provide a simple and powerful approach to endmember induction. These algorithms look for a simplex set that contains the data. Therefore, finding the endmembers is equivalent to identifying the vertices of the simplex. The vertex component analysis (VCA) algorithm [10], presents a great trade-off between performance and computational complexity. VCA iteratively projects data onto a direction orthogonal to the subspace spanned by the endmembers already determined. The new endmember signature corresponds to the extreme of the projection. The algorithm iterates until all endmembers are exhausted.

4. A STUDY CASE IN THE ALPS

We explored a case study with MODIS images in the mountainous region of the Alps. We followed the processing chain detailed in [7] and compared the use of FCLSU with respect to CLSU given a spectral library of 8 endmembers (see Fig. **??**). We also compared the use of an endmember induction algorithm before applying CLSU. In the latter case, we used the VCA algorithm. The MODIS acquisitions comprises five snow seasons: 2005-06, 06-07, 09-10, 10-11 and 11-12. After removing those images where the scene was fully covered by clouds, 854 acquisition days remained.

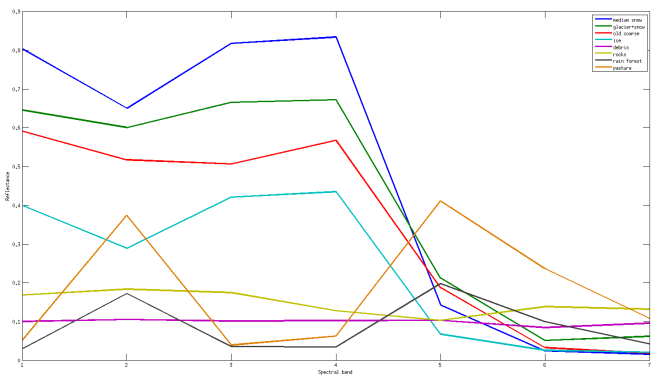

Fig. 1. Spectral library of 8 endmembers used to unmix the data.

Fig. 2 shows the average Spectral Angle Mapper (SAM), average ERGAS and average Q index reconstruction errors. These are common quality measures in unmixing literature, whereas for the former two, zero is the best value; while for the latter, one is the best. The CLSU outperforms the FCLSU in terms of reconstruction quality, and the use of CLSU with the set of endmembers induced by the VCA gives the best reconstructions. It can be noted that the errors in some acquisitions are particularly bad for the FCLSU and CLSU approaches. This is due to particularly bad climatological conditions (wide cloud covering). The EIA+CLSU approach overcomes this issue due to the adaptation of the induced endmembers to the particularities of the data.

Fig. 3 shows the average fractional abundances obtained by FCLSU and CLSU approaches respectively. It is interesting to note that the FCLSU approach reports a higher abundance of glacier snow, while the CLSU approach reports old coarse and ice instead. The peaks of 100% abundance corresponds to the cloudy acquisition days.

5. CONCLUSIONS

We have preform a preliminary study of the possibilities and challenges of using a partially constrained unmixing instead of the conventional fully constrained one, in order to address issues related to spectral variabilities. We also considered the use of endmember induction algorithms instead of a spectral library. The CLSU and the EIA+CLSU approaches results in an unmixing that fits the data better than the conventional FCLSU approach. However, the fractional abundances reported by the CLSU considerably differ from the ones reported by the FCLSU approach, where the latter reports an abundance of glacier snow, while the former reports abundances of old coarse and ice. This aspect will be further investigated by considering snow cover maps obtained from the high spatial resolution SPOT sensor and on field ground truth measures obtained by MeteoFrance. Also, the meaning of the endmembers induced by the EIA will be considered.

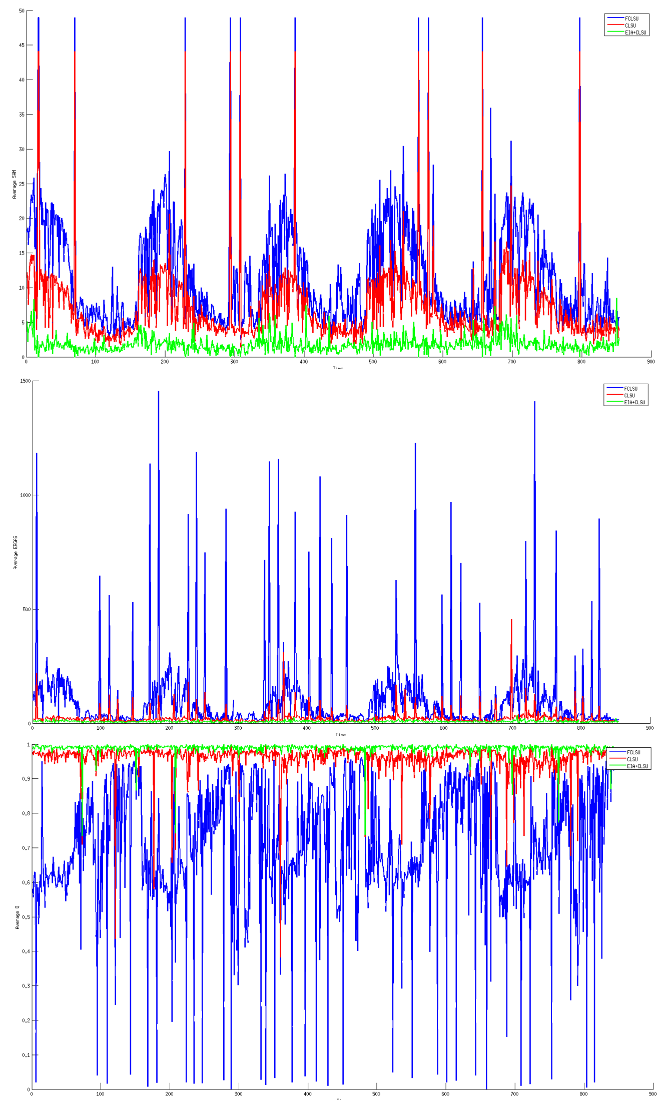

Fig. 2. Average reconstruction errors for the Arves dataset: (top) SAM, (middle) ERGAS, (bottom) Q index.

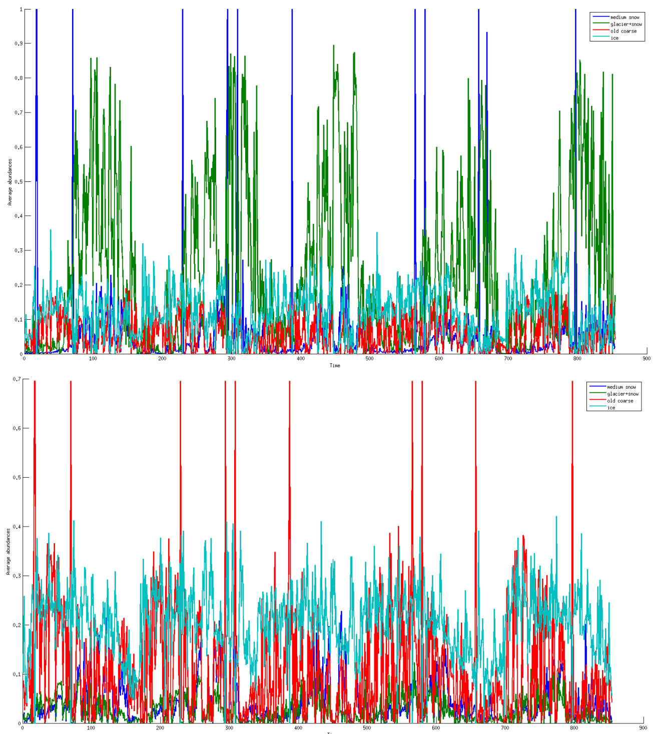

Fig. 3. Average reconstruction errors for the Arves dataset: (top) FCLSU, (bottom) CLSU.

Acknowledges

This work has been supported by a grant from Labex OSUG@2020 (Investissements d'avenir ANR10 LABX56).

6. REFERENCES

[1] V.V. Salomonson and I. Appel, "Estimating fractional snow cover from MODIS using the normalized difference snow index," *Remote Sensing of Environment*, vol. 89, no. 3, pp. 351 – 360, 2004.

[2] Thomas H. Painter, Karl Rittger, Ceretha McKenzie, Peter Slaughter, Robert E. Davis, and Jeff Dozier, "Retrieval of subpixel snow covered area, grain size, and albedo from MODIS," *Remote Sensing of Environment*, vol. 113, no. 4, pp. 868 – 879, 2009.

[3] D.K. Hall and G.A. Riggs, "Accuracy assessment of the MODIS snow products," *Hydrological Processes*, vol. 21, no. 12, pp. 1534–1547, 2007.

[4] K.R., T.H. Painter, and J. Dozier, "Assessment of methods for mapping snow cover from MODIS," *Advances in Water Resources*, vol. 51, no. 0, pp. 367 – 380, 2013.

[5] P. Sirguey, R. Mathieu, Y. Arnaud, and B.B. Fitzharris, "Seven years of snow cover monitoring with MODIS to model catchment discharge in New Zealand," in *2009 IEEE International Geoscience and Remote Sensing Symposium (IGARSS)*, 2009, vol. 2, pp. II–863–II–866.

[6] P. Sirguey, R. Mathieu, Y. Arnaud, M.M. Khan, and J. Chanussot, "Improving MODIS spatial resolution for snow mapping using wavelet fusion and ARSIS concept," *IEEE Transactions on Geoscience and Remote Sensing Letters*, vol. 5, no. 1, pp. 78–82, 2008.

[7] A. Mary, M. Dumont, J.-P. Dedieu, Y. Durand, P. Sirguey, H. Milhem, O. Mestre, H. S. Negi, A. A. Kokhanovsky, M. Lafaysse, and S. Morin, "Intercomparison of retrieval algorithms for the specific surface area of snow from near-infrared satellite data in mountainous terrain, and comparison with the output of a semi-distributed snowpack model," *The Cryosphere*, vol. 7, no. 2, pp. 741–761, 2013.

[8] A. Zare and K.C. Ho, "Endmember variability in hyperspectral analysis: Addressing spectral variability during spectral unmixing," *IEEE Signal Processing Magazine*, vol. 31, no. 1, pp. 95–104, 2014.

[9] J.M. Bioucas-Dias, A. Plaza, N. Dobigeon, M. Parente, Qian Du, P. Gader, and J. Chanussot, "Hyperspectral unmixing overview: Geometrical, statistical, and sparse regression-based approaches," *IEEE Journal of Selected Topics in Applied Earth Observations and Remote Sensing*, vol. 5, no. 2, pp. 354–379, 2012.

[10] J.M.P. Nascimento and J.M. Bioucas Dias, "Vertex component analysis: a fast algorithm to unmix hyperspectral data," *IEEE Transactions on Geoscience and Remote Sensing*, vol. 43, no. 4, pp. 898–910, 2005.